Enhancing the Radiation Pattern of Circularly Polarized Dielectric Rod Antenna Using Planar Excitation Method

IEEE Access
Multidisciplinary ⋮ Rapid Review ⋮ Open Access Journal

Received 22 September 2023, accepted 28 October 2023, date of publication 31 October 2023, date of current version 10 November 2023.

Digital Object Identifier 10.1109/ACCESS.2023.3328959

RESEARCH ARTICLE

Enhancing the Radiation Pattern of Circularly Polarized Dielectric Rod Antenna Using Planar Excitation Method

SAEED FAKHTE[1] AND LADISLAU MATEKOVITS[2,3,4], (Senior Member, IEEE)

[1]Department of Electrical and Computer Engineering, Qom University of Technology, Qom 1519-37195, Iran
[2]Department of Electronics and Telecommunications, Politecnico di Torino, 10129 Turin, Italy
[3]Istituto di Elettronica e di Ingegneria dell'Informazione e delle Telecomunicazioni, National Research Council of Italy, 10129 Turin, Italy
[4]Faculty of Electronics and Telecommunications, Politehnica University Timisoara, 300006 Timisoara, Romania

Corresponding author: Saeed Fakhte (fakhte@qut.ac.ir)

ABSTRACT In this article, by placing a teflon tube around a circularly polarized dielectric resonator antenna, a dielectric rod antenna with a directive radiation pattern is obtained. In fact, a new planar method for the excitation of circularly polarized dielectric rod antenna is proposed, which produces lower back-lobe and sidelobe levels in antenna radiation pattern compared to other planar feeding methods of circularly polarized dielectric rod antenna. It can be seen that the use of dielectric resonator inside the Teflon tube has increased the coupling of electromagnetic waves from slot aperture to dielectric rod. A prototype of the proposed antenna has been fabricated and tested, and its results are in good agreement with the simulation results. Antenna measurements display an impedance bandwidth of 15.9% from 7.96 to 9.33 GHz, an axial ratio bandwidth of 13.4% from 8 to 9.15 GHz, and a LHCP gain between 11.8 and 14.4 dB. A radiation efficiency of greater than 92% is achieved in the entire operating bandwidth of the antenna.

INDEX TERMS Dielectric rod antenna, dielectric resonator antenna, radiation pattern, planar excitation method.

I. INTRODUCTION

For many years, dielectric rods have been used in waveguide and antenna applications. They are used as waveguides because of their low losses, and they are used as antennas because of their tendency to radiate in discontinuities [1], [2]. Due to their attractive features such as wide impedance bandwidth, high directivity, high radiation efficiency and stability of the radiation pattern across the entire band, dielectric rod antennas have attracted the attention of researchers, especially in the millimetre wave and terahertz bands [3], [4]. Due to the minimal use of metal in the structure of the dielectric rod antenna, it has a high radiation efficiency and can be used in applications that require a high efficiency antenna such as millimetre wave integrated circuits [5]. The dielectric rod antenna has also been used recently in the terahertz and optical bands, due to its high radiation efficiency in these frequencies. For example, in [6], it has been coupled to a plasmonic coplanar waveguide line and appeared as an efficient optical antenna. Or in [7], the dielectric rod antenna is integrated with a photo-mixer and acts as a terahertz emitter. Recently, dielectric resonator with linear polarization has been used for feeding of linearly polarized dielectric rod antenna [8]. There exist certain distinctions between the current work and the study discussed in reference [8]. Firstly, it is important to note that the published article [8] focuses on linearly polarized dielectric rod antenna, whereas the present work explores circularly polarized dielectric rod antenna. This fundamental difference in polarization results in distinct design considerations and performance characteristics. Furthermore, the feeding mechanisms employed in the published article [8] and the present work also differ significantly. While the published article utilizes a simple slot for feeding, the present work employs a cross-slot feeding technique. This variance in feeding methods impacts the radiation pattern and impedance characteristics of the antennas. Additionally,

The associate editor coordinating the review of this manuscript and approving it for publication was Ali Karami Horestani.

it should be highlighted that the modes excited in the submitted work differ from those discussed in the published article [8]. The specific mode configurations contribute to the unique performance attributes of each design.

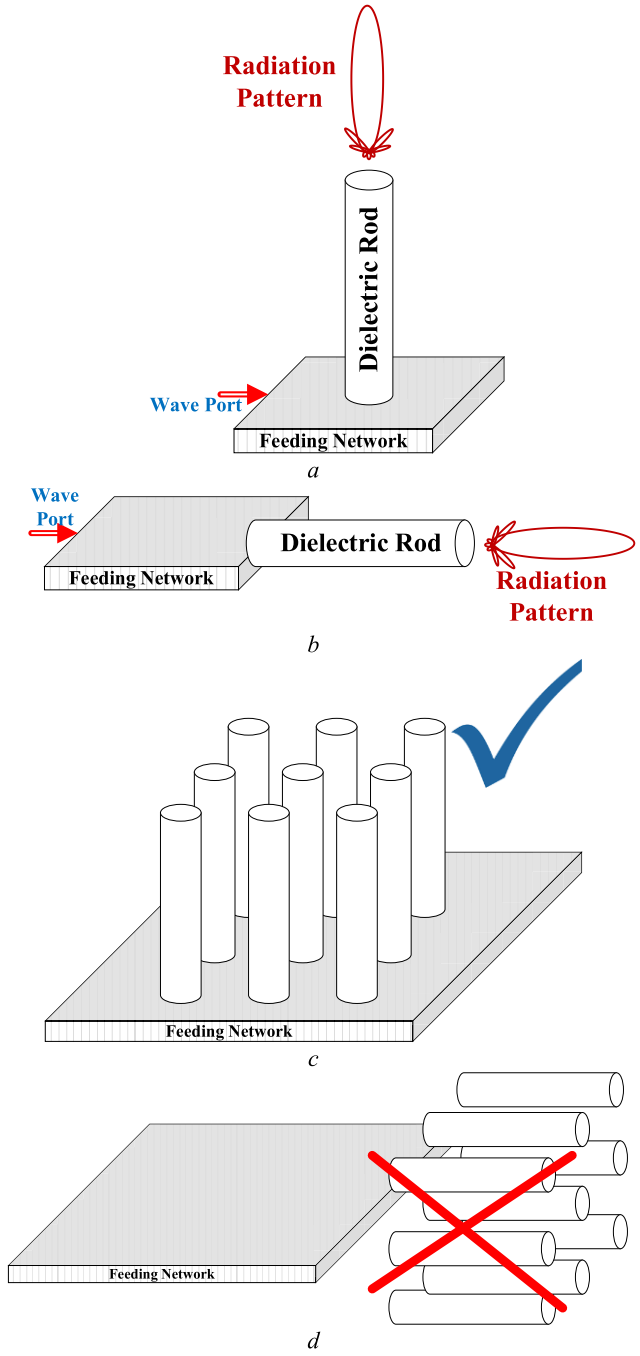

FIGURE 1. Two Different Geometries for Creating Broadside and End-Fire Patterns in Dielectric Rod Antennas, (a) Dielectric rod antenna with broadside pattern, (b) Dielectric rod antenna with end-fire pattern, (c) 2D planar array of elements with broadside pattern is easily possible, (d) 2D planar array of elements with end-fire pattern is not easily possible.

Circularly polarized antennas have been used in many telecommunication systems to reduce multipath fading and interferences [9], [10], [11], [12]. For example, their applications in satellite communication and global positioning system can be mentioned [13], [14]. Due to the interesting features mentioned before for dielectric rod antennas, they have also been used as a circular polarization radiator. Most circularly polarized dielectric rod antennas reported so far have end-fire radiation patterns. In [15], a broadband 3D-printed circularly polarized dielectric rod antenna was reported, in which an impedance bandwidth of 60.3%, an axial ratio bandwidth of 57%, and a peak gain of 11.5 dBi was attained. In [16], by rotating the dielectric rod relative to the matching cone, a circularly polarized dielectric rod antenna across the millimeter wave band was obtained. It is worth mentioning that the antenna pattern in this structure is end-fire, and the maximum radiation occurs along the substrate plane. In [17], the substrate integrated waveguide (SIW) has been used to feed the dielectric rod antenna, resulting in an impedance bandwidth of 28.3%, an axial ratio bandwidth of 25% and a maximum gain of 10.7 dB. Two antipodal cuts are engraved on the walls of an open-ended substrate integrated waveguide, which origins the radiation of two orthogonal electric field components. By adjusting the size of the cuts, the phase difference desired to generate circular polarization was also produced. Bandwidth of 41% and maximum gain of 12 dB are reported in this work [18].

In some applications, such as base station antennas, it is necessary to use a planar feeding system to excite the antenna, because otherwise, it becomes difficult to array the antennas and integrate them with microwave circuits. So far, several methods for planar excitation of dielectric rod antennas with linear polarization have been reported. In [19], folded slot aperture in the ground plane was used to couple the electromagnetic waves from the transmission line to the linearly polarized dielectric rod antenna. Also, in [20], the slot aperture excitation was used for feeding an eight-element array of dielectric rod antennas. Later, in the present work, a comparison of the slot aperture excitation method with the proposed method has been conducted.

In this work, unlike previously reported circularly polarized (CP) dielectric rod antennas that had end-fire radiation patterns, a CP dielectric rod antenna with broadside radiation pattern has been introduced thanks to a planar feeding system. In the proposed feeding system, circular polarization is generated in a rectangular dielectric resonator antenna (DRA) by placing it on a cross-slot aperture. The TE^{y}_{111} and TE^{y}_{113} orthogonal degenerate resonant modes of rectangular dielectric resonator antenna are responsible for generation of circular polarization [21].

Previously, the TE^{y}_{111} and TE^{y}_{113} modes were utilized to design a dual-band circularly polarized dielectric resonator antenna [22]. However, it is important to note that in this study, a dual-band CP DRA was employed to stimulate surface waves within the dielectric rod across a broad frequency range. This resulted in a significant increase in the gain of the antenna composed of both the dielectric rod and resonator.

For instance, in [22], the gain was 8.49 dB, whereas in this study, it reached 14 dB.

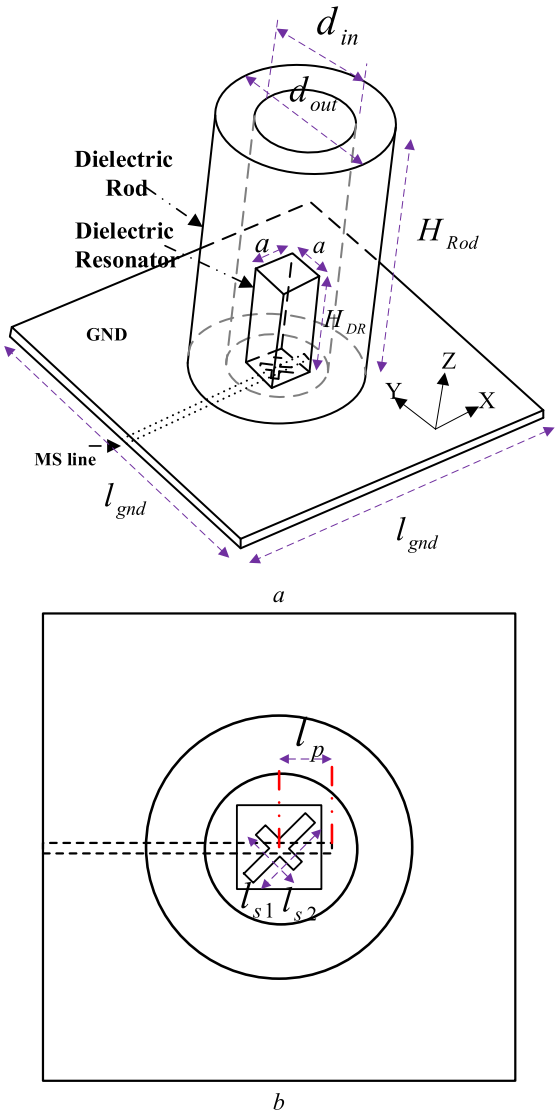

FIGURE 2. The configuration of proposed antenna (a) Perspective view, (b) Top view.

The cross slot is excited from below by the microstrip line. Then, circularly polarized degenerate modes of DRA have been coupled in the dielectric rod and propagated in it as surface waves, resulting in high-gain radiation. It is confirmed that compared to feeding with cross-slot aperture, back-lobe and side lobe levels are smaller in the proposed method.

A broadside pattern antenna produces maximum radiation in the direction perpendicular to the substrate. This is in contrast to an end-fire pattern antenna, which produces maximum radiation along the surface of the substrate.

Figure 1 illustrates the antenna configuration required to generate the broadside and end-fire radiation patterns. One advantage of using a broadside pattern antenna is that it can be easily integrated with other driving circuitry on a common printed-circuit board or a semiconductor chip using microstrip lines. This allows for high dimensional accuracy and convenient integration.

In comparison, designing a planar feeding network for a 2D array of antennas for a broadside pattern antenna can be easier than for an end-fire pattern antenna. Several methods have been reported for the planar excitation of linearly polarized dielectric rod antennas with a broadside pattern. However, to the best of the author's knowledge and based on a search of available sources, no reports have been found of a circularly polarized dielectric rod antenna with a broadside pattern and simple feeding printed on a printed circuit board (PCB).

This high gain circularly polarized antenna has various applications in the field of satellite communication, radar systems, and wireless communication. This antenna can be used for high-speed data transmission, remote sensing, and tracking applications. One of the main applications of this antenna is in satellite communication systems. It is used for transmitting and receiving signals from satellites in orbit. This antenna provides high gain and circular polarization, which helps in reducing signal loss and interference. Another application of this antenna is in radar systems. It is used for detecting and tracking objects such as aircraft, ships, and vehicles. The circular polarization of this antenna helps in reducing the effects of multipath interference and improves the accuracy of radar measurements. In wireless communication systems, this antenna is used for point-to-point links between buildings or across long distances. It provides high gain and directional radiation patterns that help in improving the signal strength and reducing interference.

The organization of the paper is as follows: in section II the geometry of the dielectric resonator fed dielectric rod antenna and the modes responsible for CP generation are discussed. In section III the measured and simulated results are investigated. Finally, in section IV the conclusion of this article is presented.

II. GEOMETRY OF ANTENNA

Figure 2 shows the geometry of the proposed circularly polarized dielectric rod antenna. Observe that a cross slot aperture with sizes of l_{s1}, l_{s2}, w_{s1}, w_{s2} is etched on the ground plane with lateral dimensions of $l_{gnd} \times l_{gnd}$. The cross-slot is excited by a microstrip line with a width of 1.15 mm and a stub length of l_p printed on the bottom side of the Rogers 4003 substrate with a thickness of 0.508 mm. Dielectric resonator with dimensions of $a \times a \times H_{DR}$ and Teflon cylindrical tube as

TABLE 1. The optimized values of the proposed antenna. unit: mm.

parameter	H_{DR}	H_{ROD}	d_{in}	d_{out}	l_{gnd}
value	19	74	16	28	60
parameter	l_{s2}	l_{s1}	a	l_p	
value	7.6	5.1	7.1	1.9	

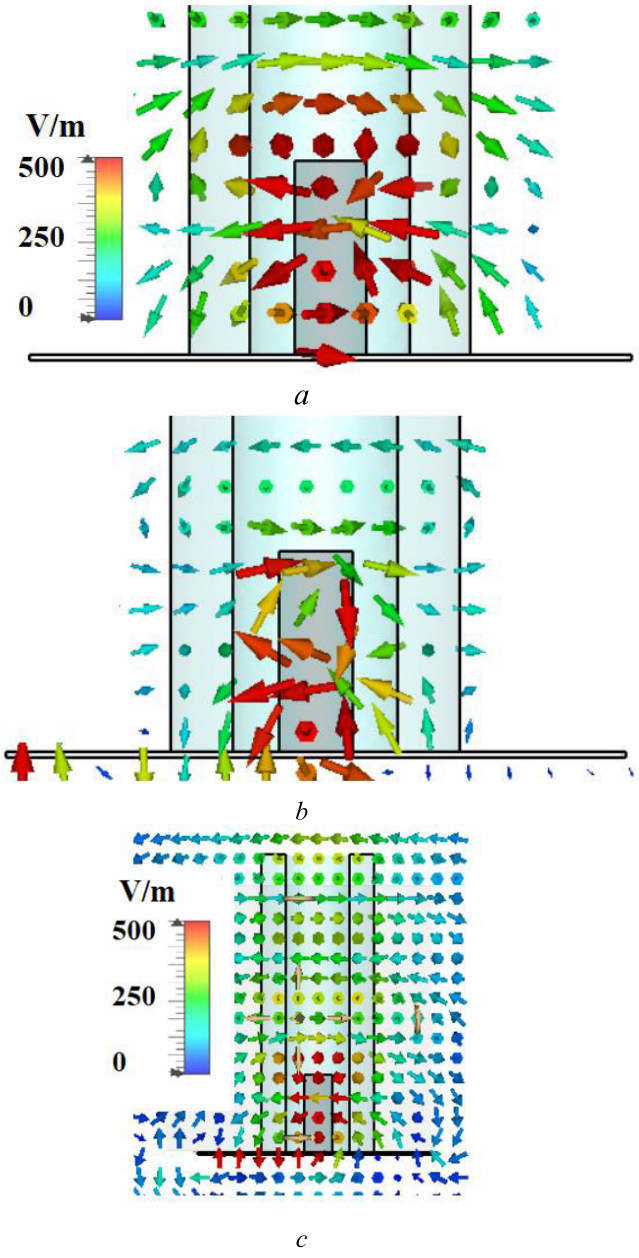

FIGURE 3. The electric field distribution at different frequencies (a) at 8 GHz in the zoomed area, encompassing the dielectric resonator, (b) at 8.7 GHz in the zoomed area, encompassing the dielectric resonator, (c) at 8.5 GHz within the whole antenna.

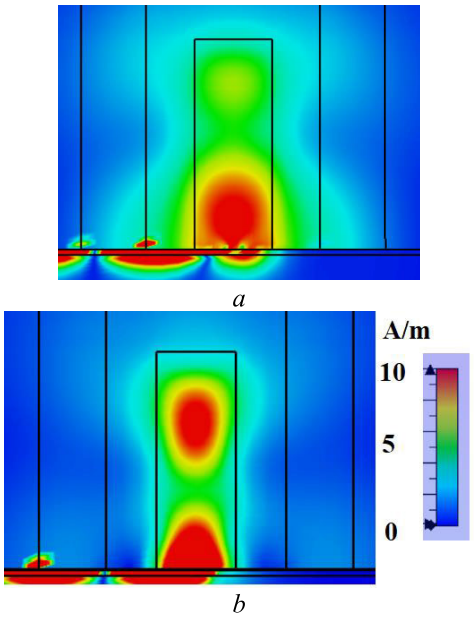

FIGURE 4. The magnetic field distribution at different frequencies (a) at 8 GHz, (b) at 8.7 GHz.

dielectric rod with inner and outer diameters of d_{in} and d_{out} and height of H_{Rod} are placed on the ground plane.

The dielectric resonator is made of Rogers 6010 substrate ($\varepsilon_r = 10.2, tan\delta = 0.002$) and the dielectric rod is made of Teflon ($\varepsilon_r = 2.1$). The dimensions of the dielectric resonator are calculated in such a way that the resonance frequencies of the TE^y_{111} and TE^y_{113} modes are 8 and 8.6 GHz, respectively.

When designing the proposed antenna, it's important to note that its functional bandwidth is determined by the resonances of the dielectric resonator modes. Placing a Teflon tube around the dielectric resonator has a slight effect on the antenna's reflection coefficient, but the frequencies at the beginning and end of the impedance band remain largely unchanged. As such, the resonance frequency formulas for the TE^y_{111} and TE^y_{113} modes of a rectangular dielectric resonator antenna can be used in the design process.

The design process for this antenna involves several steps. In the first step, it is assumed that there is no Teflon tube and the goal is to design a rectangular dielectric resonator antenna with circular polarization radiation. To calculate the resonance frequencies of the DRA TE^y_{mnp} modes, the following formulas are used [21], [22]:

$$\begin{cases} k_y a = 2\tan^{-1}\left(\dfrac{\sqrt{(\varepsilon_r - 1)\,k_o^2 - k_y^2}}{k_y}\right) \\ +(\mathrm{n}-1)\pi \\ k_x^2 + k_y^2 + k_z^2 = \varepsilon_r k_o^2 \end{cases}$$
$$k_x = \frac{m\pi}{a}, k_z = \frac{p\pi}{2H_{DR}}, k_0 = 2\pi f_0/c \quad (1)$$

where the length and width of DRA is equal to a and its height is equal toH_{DR}, c is the speed of light in vacuum and ε_r is the dielectric constant of the dielectric resonator. In the above equation, k_0 and k_y can be obtained by solving a system of two equations with two unknowns. The resonant frequency of the mode can then be calculated using k_0. Given a value of 7.1 mm for a and 19mm for H_{DR}, the resonance frequencies for the TE^y_{111} and TE^y_{113} modes are calculated to be 8 and 8.6 GHz, respectively.

To proceed, the DRA is encased with a Teflon tube, which is carefully designed and positioned. The diameter of the tube is determined by selecting a value between d_{min} and d_{max},

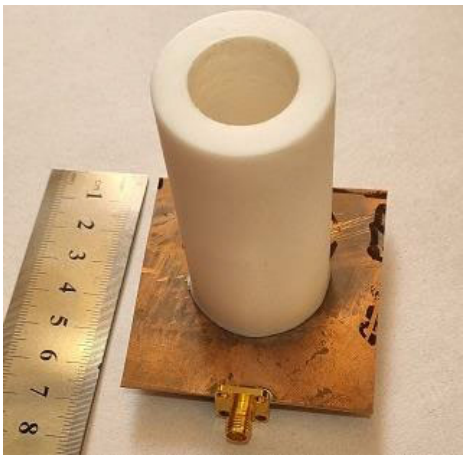

FIGURE 5. The fabricated prototype of the proposed CP antenna.

while the initial length is set at $2\lambda_0$ [23], [24].

$$d_{\max} \approx \frac{\lambda_0}{\sqrt{\pi\,(\varepsilon_r - 1)}} \tag{2}$$

$$d_{\min} \approx \frac{\lambda_0}{\sqrt{2.5\pi\,(\varepsilon_r - 1)}} \tag{3}$$

where λ_0 is the free space wavelength corresponding to the middle frequency of the band. Thus, based on the central frequency of 8.65 GHz, it is recommended that the diameter of the tube falls within the range of 11.3 to 17.9 mm. Additionally, the initial value for the tube's length is set to 70 mm.

To further enhance the antenna's performance, the next step involves utilizing CST software to optimize its Left-Hand Circular Polarization (LHCP) gain, minimize side lobe level (SLL), and maximize impedance bandwidth.

To calculate the resonance frequencies of these modes, the theoretical formulas of the dielectric waveguide model (DWM) method have been used [21] and [26]. DWM, or Dielectric Waveguide Model, is a widely recognized method used to determine the electric and magnetic fields within a dielectric resonator, as well as calculate the resonance frequencies of its TE modes [26].

The dimensions of this antenna have been optimized with the aim of achieving the best impedance bandwidth, 3 dB axial ratio bandwidth, gain and side lobe levels and are listed in Table 1. The optimization process has started with the parametric study of the antenna. Then, by swiping the parameters around the values of this step, the best possible results have been obtained by the CST software optimization algorithms.

The values of the inner and outer radii of the dielectric rod have been obtained considering that there is only single-mode propagation in this structure.

Figure 3 illustrates the electric field vector distribution in the zoomed area, encompassing the dielectric resonator, as well as the overall electric field distribution within the antenna structure.

The electric field vector distribution of the proposed antenna at frequencies of 8 and 8.7 GHz and its electric

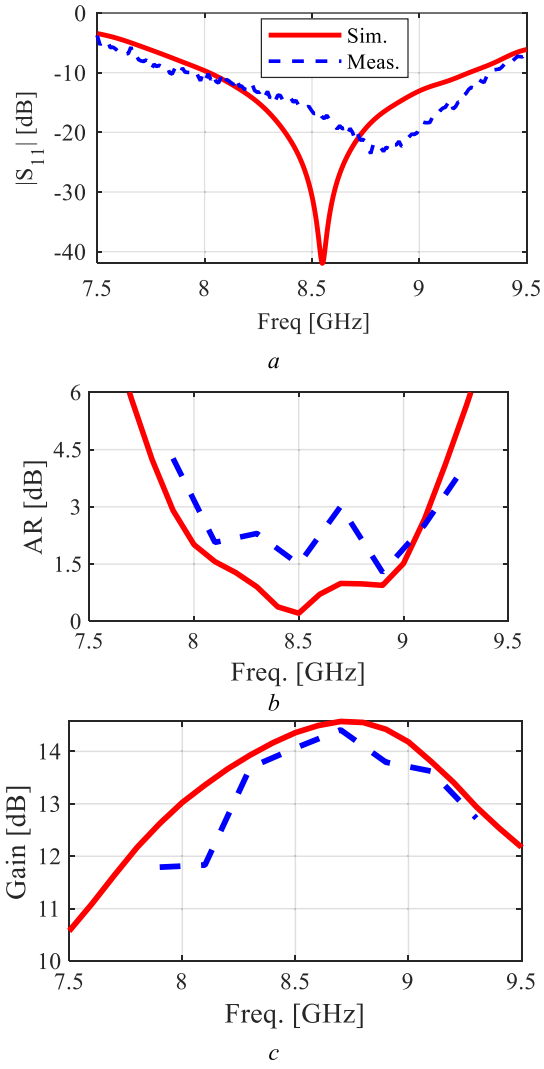

FIGURE 6. The Measured and simulated results of the proposed CP antenna. (a) Reflection Coefficient, (b) Axial ratio, and (c) LHCP gain.

field magnitude distribution at the frequency of 8.5 GHz are shown in Figure 3. The vector distributions shown in Figures 3a and b indicate that TE_{111} and TE_{113} modes of the rectangular dielectric resonator antenna resonate at frequencies of 8 and 8.7 GHz, respectively. It can also be understood from Figure 3c that the surface wave fields are excited in the dielectric rod.

The transfer of power between the antenna and port is affected by the position and type of the port in relation to the antenna. Although numerical methods are typically necessary to determine these values, knowledge of the field distributions inside the rod and application of the Lorentz Reciprocity Theorem can offer valuable insights. The source can be represented as either an electric or magnetic current, and by using appropriate boundary conditions with the reciprocity theorem, one can determine the amount of coupling, χ, between the source and dielectric rod fields. The coupling amount for electric and magnetic sources can be computed

using following equations [26].

$$\chi \propto \int_V (\boldsymbol{E}_{ROD} \cdot \boldsymbol{J}_s)\, dV \tag{4}$$

$$\chi \propto \int_V (\boldsymbol{H}_{ROD} \cdot \boldsymbol{M}_s)\, dV \tag{5}$$

The electric and magnetic current sources are denoted by J_s and M_s, respectively, while the electric and magnetic fields within the dielectric rod are represented by E_{ROD} and H_{ROD}. The volume in which the electric and/or magnetic current sources exist is indicated by V.

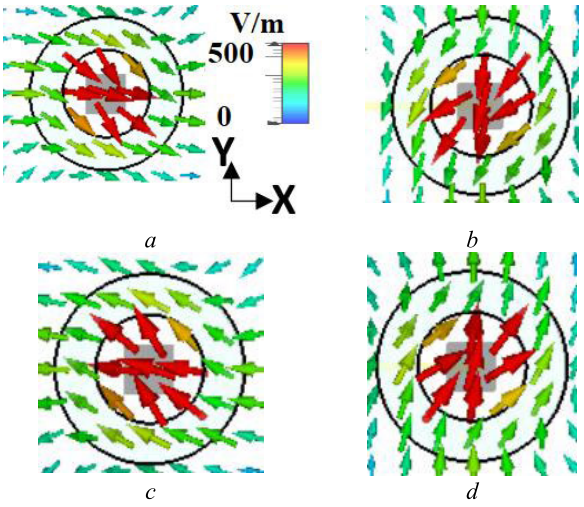

FIGURE 7. The vector electric field distribution of fundamental mode of CP dielectric rod antenna at 8.5 GHz for various phases of the feeding (a)0 deg., (b) 90 deg., (c) 180 deg., (d) 270 deg.

Equation (4) suggests that for a robust connection with an electric current source, it is necessary to position the source in a region of the DRA with potent electric fields. On the other hand, equation (5) indicates that to establish a strong bond with a magnetic current source like an aperture or loop, it is essential to place the source in an area with intense magnetic fields.

An aperture slot can be considered as a source of magnetic current. Figure 4 depicts the magnetic field distribution of $TE^{x,y}_{111}$ and $TE^{x,y}_{113}$ modes of dielectric resonator antenna.

The graph clearly illustrates that the magnetic field intensity is particularly concentrated at the ground plane of the antenna. Therefore, by placing a slot in this location, it is possible to create optimal coupling between the transmission line and DRA.

The proposed antenna utilizes cross slot aperture coupling to generate circular polarization radiation through the excitation of two degenerate modes, namely TE^{x}_{111} and TE^{y}_{111} modes of dielectric resonator. Circular polarization requires two perpendicular electric field components with a phase difference of 90 degrees. These orthogonal components are produced by the aforementioned modes. Additionally, the phase difference of 90 degrees is achieved by incorporating two unequal length orthogonal slots that form a cross slot.

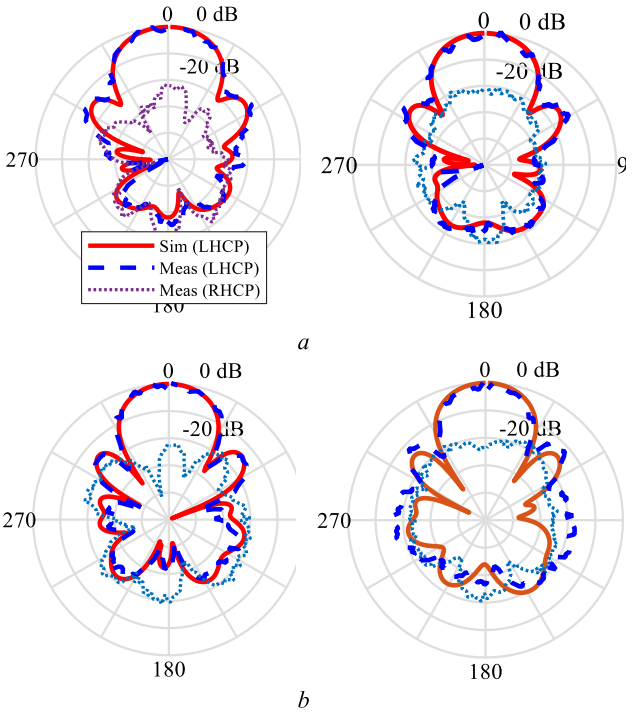

FIGURE 8. The measured and simulated LHCP and RHCP radiation patterns of the proposed CP antenna. (a) at 8.3 GHz, (b) at 8.8 GHz.

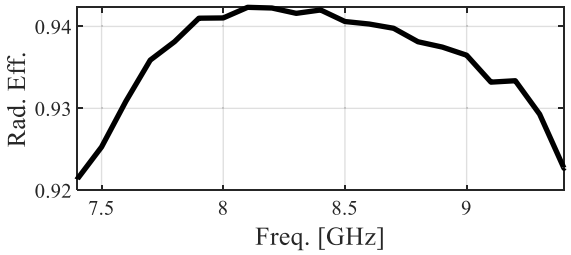

FIGURE 9. The simulated radiation efficiency of the proposed CP dielectric rod antenna.

To achieve circular polarization in the antenna, two slots intersecting in a cross manner with lengths of ls1 and ls2 have been utilized, as illustrated in Figure 2. In this study, the longer slot is positioned at an angle of $\varphi = +45$ degrees while the shorter slot is placed at an angle of φ =-45 degrees, resulting in the production of left-handed circular polarization. If the position of the two slots is altered, such that the longer slot is located at an angle of φ =-45 degrees and the shorter slot is positioned at an angle of $\varphi = +45$ degrees, right-handed circular polarization is produced.

The cross-slot aperture excites two pairs of $TE^{x,y}_{111}$ and $TE^{x,y}_{113}$ modes at two distinct frequencies. These modes produce electric field components that are perpendicular to each other and have nearly equal amplitudes. By adjusting the length of the orthogonal slots, a phase difference of 90 degrees is achieved, resulting in circular polarization. The orientation of the longer slot determines whether the circular polarization is LHCP or Right-Hand Circular Polar-

ization (RHCP), with the direction of rotation indicating the polarization mode of the antenna when viewed from above.

III. RESULTS AND DISCUSSION

A prototype of the proposed CP dielectric rod antenna has been fabricated and can be seen in Figure 5. The fabricated antenna consists of a Rogers RO4003 substrate, a Teflon tube and a rectangular dielectric resonator. The input port of the antenna can be connected to the coaxial cable by the SubMiniature version A (SMA) connector.

A vector network analyzer (VNA) has been used to test the reflection coefficient of the antenna, the result of which is displayed in Figure 6. The measurement results of axial ratio and gain are also presented in this figure. The reflection coefficient diagram shows an impedance bandwidth of 15.9% (7.96 to 9.33 GHz). The measured and simulated reflection coefficients have some discrepancy, which seems normal considering the fabrication and measurement errors, especially in this frequency band where the sizes are relatively small. As shown in Figure 6b, a 3-dB axial ratio bandwidth of 13.4% is obtained from the frequency of 8 to 9.15 GHz, which completely overlaps with the impedance bandwidth of the antenna. Figure 6c shows the LHCP gain diagram of the antenna, where the LHCP gain varies between 11.8 and 14.4 dB. Observe that the peak gain of the combined structure of dielectric resonator and dielectric rod reaches 14.4 dB, which is much higher than the usual gain of dielectric resonator antennas, which is often below 9 dB.

The electric field distribution in the XoY plane view of the dielectric rod antenna at the frequency of 8.5 GHz is shown in Figure 7. The rotation of the electric field vector is evident by varying the phase of the input feed source from 0 to 270 degrees, which confirms the generation of LHCP circular polarization in the antenna.

The left hand circularly polarized (LHCP) radiation patterns of the proposed antenna at two frequencies of 8.3 and 8.8 GHz are displayed in Figure 8. Back lobe level below -20 dB, side lobe level below -12 dB and cross polar discrimination better than 20 dB are evident in the patterns.

A good agreement is observed between the simulation and measurement results. The diagram of the radiation efficiency of the proposed antenna is drawn in Figure 9, which shows an efficiency of more than 92% in the entire band. This high efficiency in these frequencies is due to minimal use of metal in the antenna structure.

Finally, the CP dielectric rod antenna with the proposed feeding has been compared with the one excited only by the cross-slot. Figure 10 shows the comparison of reflection coefficients, axial ratios, gains and side lobe levels of these two antennas. The superiority of the dielectric rod antenna excited by the proposed feeding method to the antenna excited only by cross-slot is evident, especially in the gain and side lobe levels diagrams.

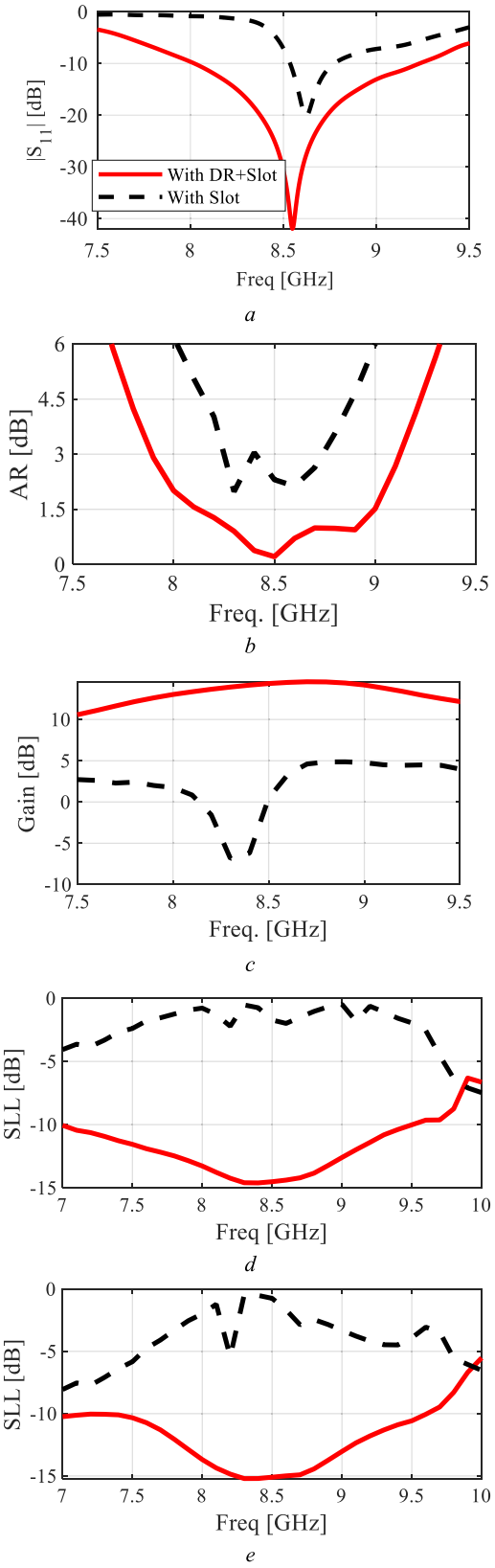

FIGURE 10. The comparison between the simulated results of the dielectric resonator fed dielectric rod antenna and slot fed dielectric rod antenna (a) reflection coefficient, (b) axial ratio, (c) gain, (d) side lobe level in XoZ plane, and (e) side lobe level in YoZ plane.

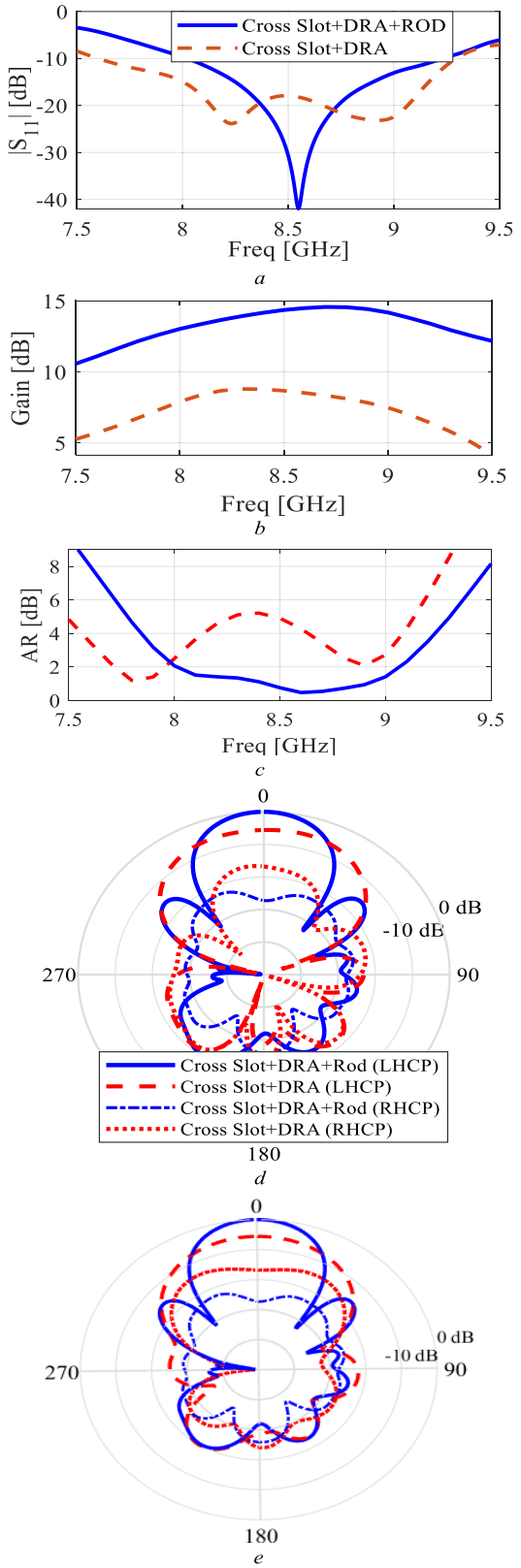

FIGURE 11. The comparison between the simulated results of slot fed dielectric resonator antenna and the proposed dielectric rod antenna, (a) Reflection coefficient, (b) LHCP gain, (c) Axial ratio, (d) Gain patterns at 8.5 GHz in XoZ plane, (e) Gain patterns at 8.5 GHz in YoZ plane.

It can be understood from these diagrams that the cross-slot alone is not able to properly launch the surface waves inside the rod.

In Table 2, the proposed CP antenna has been compared with several other CP dielectric rod antennas with both end-fire and broadside patterns. As mentioned earlier, the main advantage of this antenna over previous works is its broadside pattern and relatively simpler planar feeding. Upon reviewing the literature, only one example of a CP dielectric rod antenna with a broadside pattern was found, as shown in Table 2 [25]. Compared to the present work, its results show narrower axial ratio and impedance bandwidths and a more complex feeding system that uses a metallic waveguide to feed the antenna. Its gain is higher compared to the proposed antenna, which can be attributed to its length being almost three times greater. In comparison to the other works listed in the Table 2 that exhibit an end-fire pattern [15], [16], [17], [18], this antenna demonstrates a higher gain despite its shorter electrical length. Nonetheless, as mentioned earlier, the proposed structure's ability to be utilized in 2D planar arrays is among its primary advantages when compared to previously reported works. Table 2 indicates that the proposed structure utilizes PCB manufacturing technology, which is less complex in comparison to structures [15], [16], [18], and [25] that employ metal machining technology.

The higher bandwidth of the proposed antenna, in comparison to the antenna reported in [25], can be attributed to two main factors. Firstly, dielectric resonator antennas typically exhibit a larger bandwidth when compared to patch antennas [26]. So, when employing the dielectric resonator as the feeding mechanism for the dielectric rod antenna, a broader band antenna can be achieved when compared to the patch-fed dielectric rod antenna. Furthermore, two radiation modes of the dielectric resonator, specifically TE^x_{111} and TE^x_{113}, as well as their corresponding degenerate resonant modes, TE^y_{111} and TE^y_{113} are excited. This multi-mode excitation contributes to a broader bandwidth in comparison to a single-mode patch antenna. As a result, these combined factors contribute to the observed higher bandwidth in the proposed dielectric resonator antenna.

The higher gain observed in the patch-fed dielectric rod antenna, in comparison to the proposed antenna, can be attributed to a couple of key factors. Firstly, the utilization of a metal waveguide surrounding the rod and patch in the patch-fed dielectric rod antenna has led to an increase in antenna gain. This metal waveguide helps to confine and guide the electromagnetic energy, resulting in improved radiation efficiency and higher gain. Additionally, the length of the patch-fed rod antenna is approximately 6.2 times the wavelength, which contributes to enhanced directivity and focused radiation. In contrast, the proposed antenna has a length of about 2.13 times the wavelength, which may result in comparatively lower directivity. These differences in antenna length directly impact the spatial

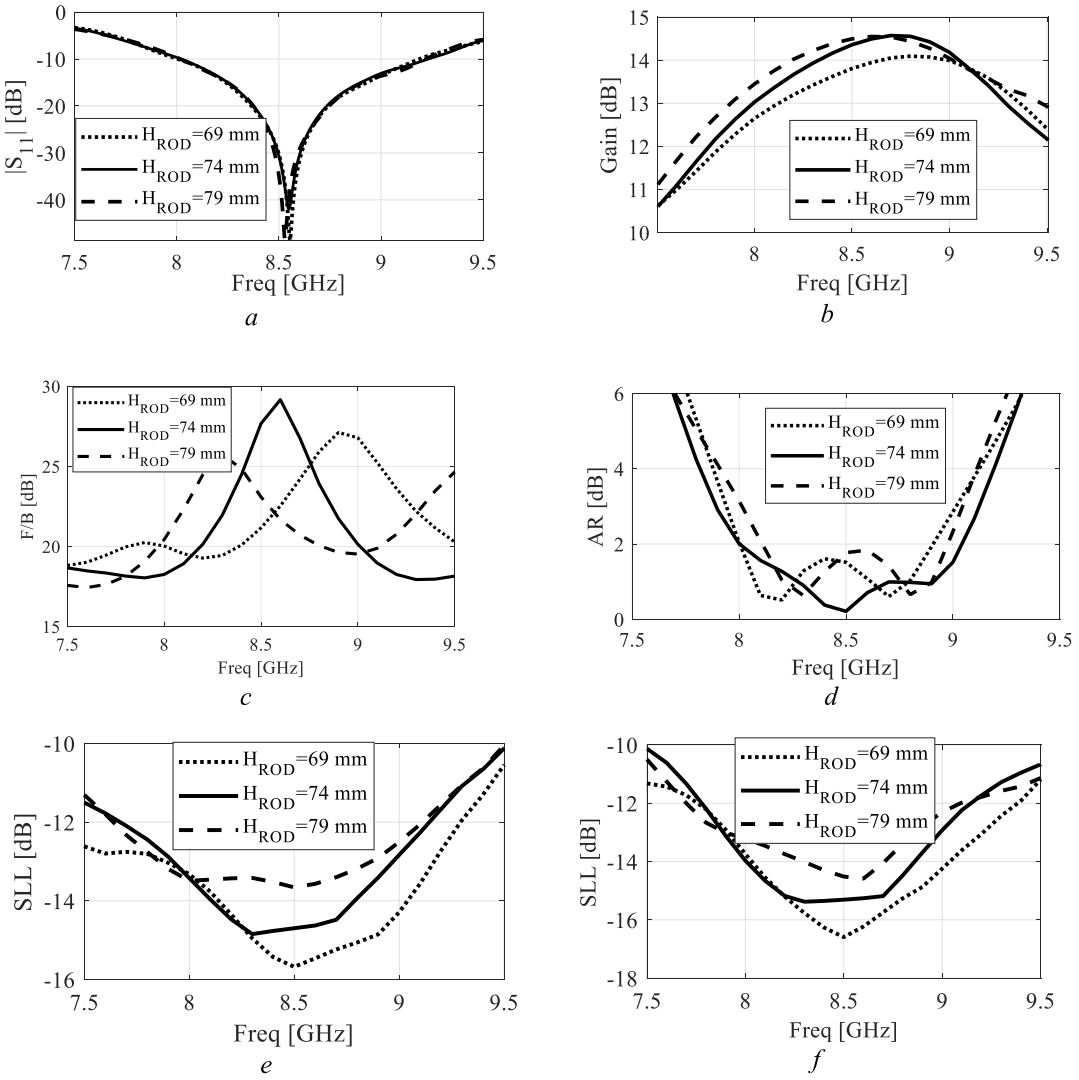

FIGURE 12. The simulated results of the proposed CP dielectric rod antenna for various height, H_{ROD}, (a) reflection coefficient, (b) gain, (c) axial ratio, (d) front-to-back ratio, (e) side lobe level in XoZ plane, (f) side lobe level in YoZ plane.

distribution of the radiated energy, ultimately affecting the gain performance.

The large volume and high height of the dielectric resonator antenna play a significant role in achieving good directivity. These characteristics enable a strong coupling of electromagnetic fields to the rod, allowing for a higher concentration of radiated energy in the desired direction. As a result, the dielectric resonator antenna exhibits improved directivity.

It is worth noting that the axial ratio and impedance bandwidths of the proposed antenna can be enhanced by utilizing a broadband dielectric resonator, as opposed to the basic rectangular dielectric resonator employed in this study.

Figure 11 compares the reflection coefficient and LHCP gain results of the proposed CP dielectric resonator antenna with and without the Teflon tube. The goal is to investigate the effect of the Teflon tube on the antenna's performance. As shown in Figure 11 (a) and (b), removing the Teflon tube slightly improves the impedance bandwidth but significantly decreases the LHCP gain. Thus, adding a Teflon tube to the CP dielectric resonator increases the antenna's gain by about 6dB. It should be noted that the addition of teflon tube slightly changes the axial ratio and SLL, which is not significant, so its graphs are not added. Figures 11 (d) and (e) showcase the radiation patterns of the resulting antennas in the XoZ and YoZ planes, respectively. These figures effectively demonstrate the narrowing of the main beam of the final antenna as compared to the dielectric resonator antenna.

Figure 12 illustrates the variations in reflection coefficient, LHCP gain, axial ratio, front-to-back ratio, and side lobe levels in two XoZ and YoZ planes of the antenna radiation pattern for different values of dielectric rod height (H_{ROD}). The figure indicates that a change of 5 mm in rod height around the optimal value of 74 mm does not significantly affect the reflection coefficient and axial ratio. However,

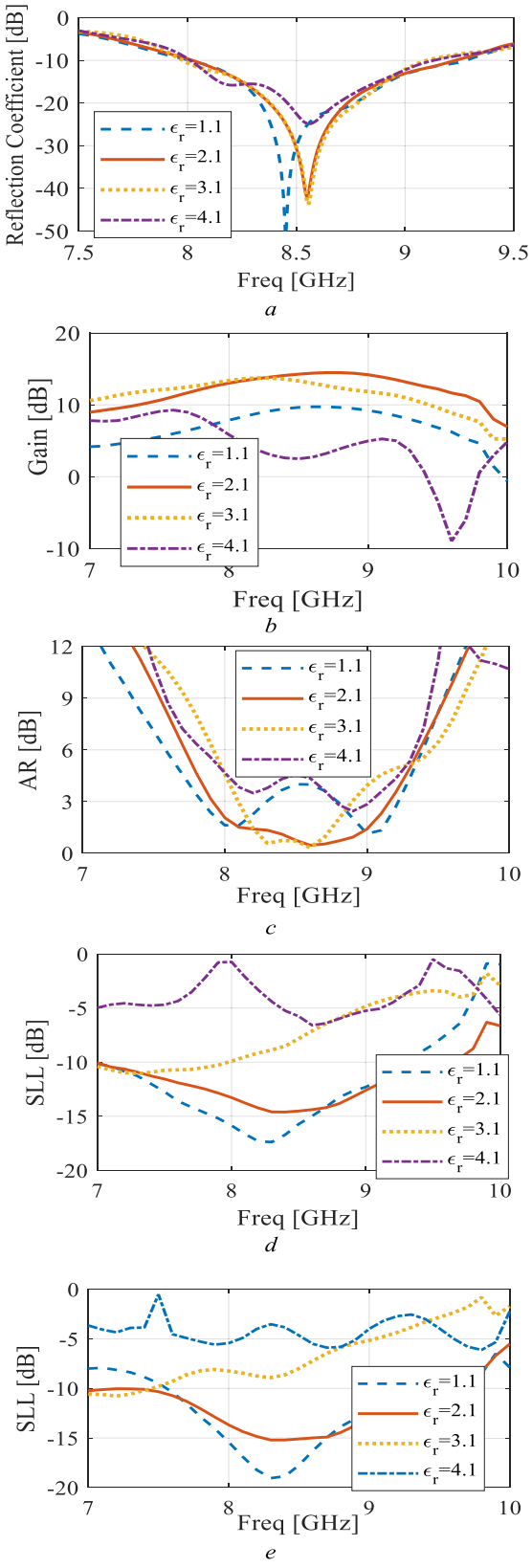

FIGURE 13. The simulated results of the proposed CP dielectric rod antenna for various permittivity of tube, (a) reflection coefficient, (b) gain, (c) axial ratio, (d) side lobe level in XoZ plane, (e) side lobe level in YoZ plane.

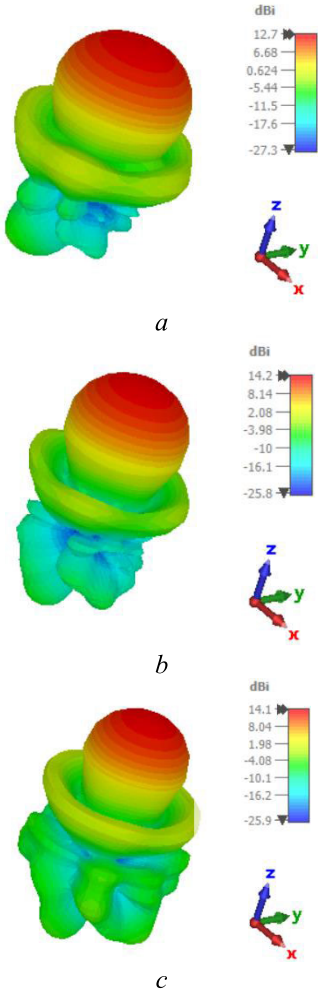

FIGURE 14. The Simulated 3D radiation patterns of the proposed antenna, (a) at 8 GHz, (b) at 8.5 GHz, and (c) at 9 GHz.

it has a significant impact on LHCP gain, F/B, and SLLs. The gain increases with an increase in rod height, but to achieve a balance between F/B, gain, and SLLs, the most suitable choice is $H_{ROD} = 74mm$.

Figure 13 demonstrates the impact of varying tube permittivity on reflection coefficient, LHCP gain, axial ratio, and side lobe levels in two XoZ and YoZ planes of the antenna radiation pattern. The results indicate that altering the permittivity from 1.1 to 4.1 does not significantly affect the impedance bandwidth of the antenna. However, it has a drastic effect on the other graphs. The optimal solution is achieved with an ε_r value of 2.1, which corresponds to the Teflon material utilized in this study.

The 3D radiation patterns of the proposed antenna at 8, 8.5, and 9 GHz are depicted in Figure 14. It is evident from the figures that the antenna exhibits a broadside radiation pattern across its entire operating band.

To improve the clarity of the design process for the proposed antenna, a flowchart similar to the one reported in [27] is presented in Figure 15.

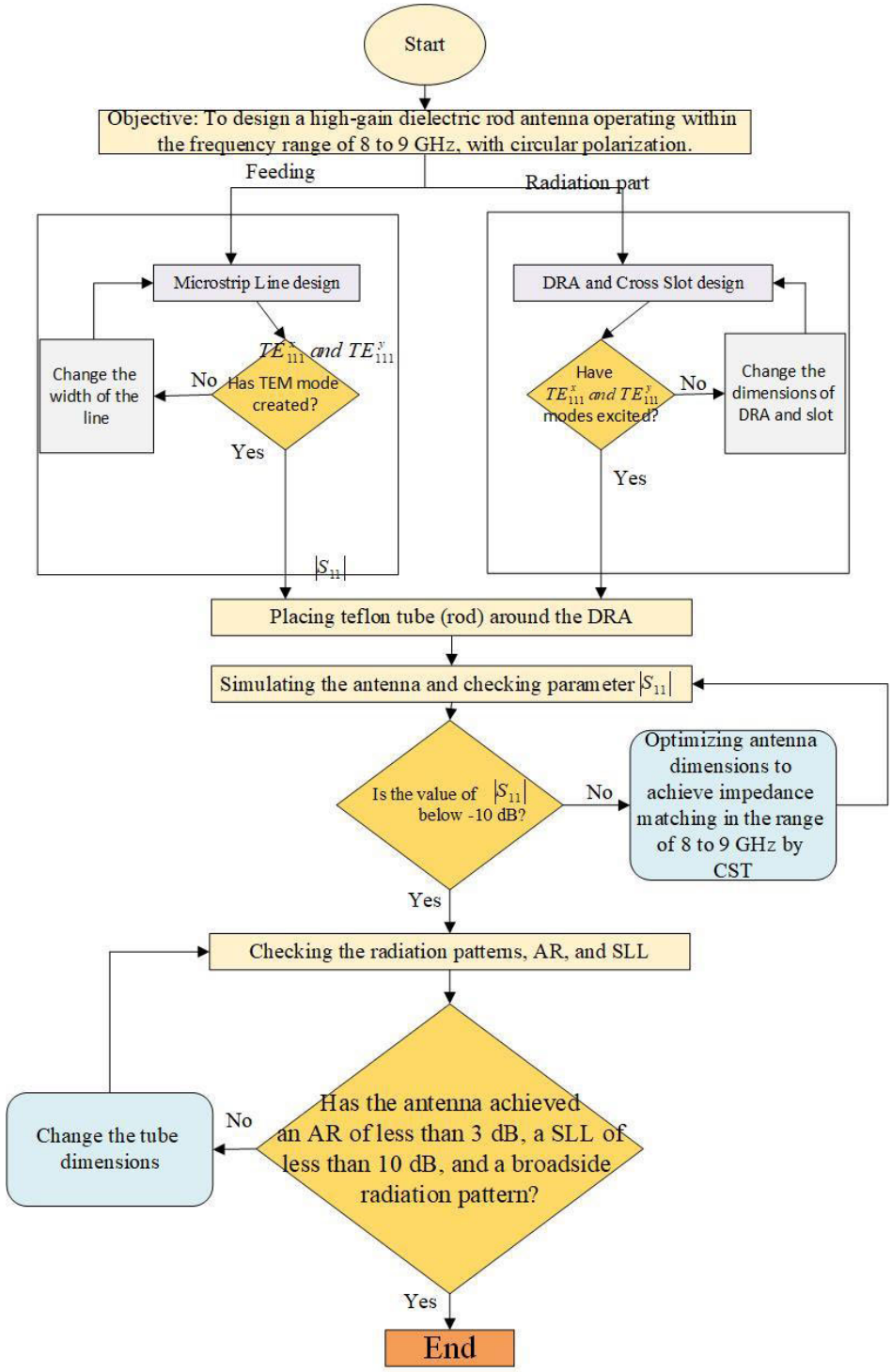

FIGURE 15. Flowchart of proposed antenna design.

The circularly polarized dielectric rod antenna discussed in this article offers a range of benefits, making it suitable for various applications, including medical devices, ground exploration radars, and military industries. Its wide impedance bandwidth and high gain contribute to its versatility. Additionally, this antenna can be utilized for high-power radiation to effectively target and treat tumors in the body. Its directional pattern and wide band capabilities make it particularly well-suited for this application. Moreover, in the microwave frequency range, it can serve as a

TABLE 2. Comparison with cp dielectric rod antennas.

Ref.	pattern	Feeding system	IBW (%)	ARBW (%)	Gain [dB]	Length	Processing technology
[15]	End-fire	Metallic Waveguide	60.3	57	8.3~11.5	$3.5\lambda_0$	Metal machining+3D printing
[16]	End-fire	Metallic Waveguide	>37	37	9~10	$4.3\lambda_0$	Metal machining
[17]	End-fire	SIW	28.3	25	9~10.7	$5.08\lambda_0$	PCB
[18]	End-fire	Metallic Waveguide	52.9	41	10.1~12.9	$6.4\lambda_0$	Metal machining+PCB
[25]	Broadside	Metallic Waveguide+ Patch	6	2.7	15~16.74	$6.2\lambda_0$	Metal machining+PCB
This work	Broadside	Dielectric resonator+Slot	15.9	13.4	11.8~14.4	$2.13\lambda_0$	PCB

λ_0 is the wavelength that corresponds to the central frequency of the antenna's frequency band.

feed for the reflector antenna, enhancing the performance of the system. Furthermore, it has potential uses in microwave sensors, further expanding its utility [28], [29], [30], [31].

IV. CONCLUSION

In this article, a novel method for planar excitation of dielectric rod antenna with circular polarization is presented. In the previously reported works, circularly polarized dielectric rod antennas all had end-fire radiation patterns, but in this work, a broadside pattern is obtained. In other words, the direction of the main lobe of the radiation pattern of the proposed antenna is normal to the ground plane, which makes it possible to use it in planar arrays. A prototype of the proposed antenna has been fabricated and its test results show an impedance bandwidth of 15.9%, an axial bandwidth ratio of 13.4% and a maximum gain of 14.4 dB. Also, the simulation and measurement results are in good agreement.

REFERENCES

[1] S. Kobayashi, R. Mittra, and R. Lampe, "Dielectric tapered rod antennas for millimeter-wave applications," *IEEE Trans. Antennas Propag.*, vol. AP-30, no. 1, pp. 54–58, Jan. 1982, doi: 10.1109/TAP.1982.1142758.

[2] R. Kazemi, A. E. Fathy, and R. A. Sadeghzadeh, "Dielectric rod antenna array with substrate integrated waveguide planar feed network for wideband applications," *IEEE Trans. Antennas Propag.*, vol. 60, no. 3, pp. 1312–1319, Mar. 2012, doi: 10.1109/TAP.2011.2182489.

[3] N. Hirayama, A. Nakayama, H. Yoshikawa, T. Shimizu, and Y. Kogami, "Measurement technique for interface and surface conductivities at millimeter-wave frequencies using dielectric rod resonator excited by nonradiative dielectric waveguide," *IEEE Trans. Microw. Theory Techn.*, vol. 70, no. 5, pp. 2750–2761, May 2022, doi: 10.1109/TMTT.2022.3157301.

[4] Y. Chen, L. Zhang, Y. He, C. Mao, S.-W. Wong, W. Li, P. Chu, and S. Gao, "Broadband high-gain SIW horn antenna loaded with tapered multistrip transition and dielectric slab for mm-wave application," *IEEE Trans. Antennas Propag.*, vol. 70, no. 7, pp. 5947–5952, Jul. 2022, doi: 10.1109/TAP.2022.3161349.

[5] A. Patrovsky and K. Wu, "94-GHz planar dielectric rod antenna with substrate integrated image guide (SIIG) feeding," *IEEE Antennas Wireless Propag. Lett.*, vol. 5, pp. 435–437, 2006, doi: 10.1109/LAWP.2006.885014.

[6] E. Ahmadi, S. Fakhte, and S. S. Hosseini, "Dielectric rod nanoantenna fed by a planar plasmonic waveguide," *Opt. Quantum Electron.*, vol. 55, no. 2, p. 115, Dec. 2022, doi: 10.1007/s11082-022-04409-w.

[7] A. Rivera-Lavado, S. Preu, L. E. García-Muñoz, A. Generalov, J. Montero-de-Paz, G. Döhler, D. Lioubtchenko, M. Méndez-Aller, F. Sedlmeir, M. Schneidereit, H. G. L. Schwefel, S. Malzer, D. Segovia-Vargas, and A. V. Räisänen, "Dielectric rod waveguide antenna as THz emitter for photomixing devices," *IEEE Trans. Antennas Propag.*, vol. 63, no. 3, pp. 882–890, Mar. 2015, doi: 10.1109/TAP.2014.2387419.

[8] S. Fakhte, "A new planar feeding method of dielectric rod antenna using dielectric resonator," *Sci. Rep.*, vol. 13, no. 1, p. 9242, Jun. 2023, doi: 10.1038/s41598-023-36543-0.

[9] S. S. Gao, Q. Luo, and F. Zhu, *Circularly Polarized Antennas*. Hoboken, NJ, USA: Wiley, 2014.

[10] C. Lee, T. V. Hoang, S. W. Chi, S. Lee, and J. Lee, "Low profile quad-beam circularly polarised antenna using transmissive metasurface," *IET Microw., Antennas Propag.*, vol. 13, no. 10, pp. 1690–1698, May 2019, doi: 10.1049/iet-map.2018.6056.

[11] G. Varshney, "Gain and bandwidth enhancement of a singly-fed circularly polarised dielectric resonator antenna," *IET Microw., Antennas Propag.*, vol. 14, no. 12, pp. 1323–1330, Oct. 2020, doi: 10.1049/iet-map.2019.0932.

[12] K. Ding, R. Hong, D. Guan, L. Liu, and Y. Wu, "Broadband circularly polarised stacked antenna with sequential-phase feed technique," *IET Microw., Antennas Propag.*, vol. 14, no. 8, pp. 779–784, Apr. 2020, doi: 10.1049/iet-map.2019.0894.

[13] Y. Zhou, C.-C. Chen, and J. L. Volakis, "Single-fed circularly polarized antenna element with reduced coupling for GPS arrays," *IEEE Trans. Antennas Propag.*, vol. 56, no. 5, pp. 1469–1472, May 2008, doi: 10.1109/TAP.2008.922887.

[14] B. Liang, B. Sanz-Izquierdo, E. A. Parker, and J. C. Batchelor, "A frequency and polarization reconfigurable circularly polarized antenna using active EBG structure for satellite navigation," *IEEE Trans. Antennas Propag.*, vol. 63, no. 1, pp. 33–40, Jan. 2015, doi: 10.1109/TAP.2014.2367537.

[15] J. Huang, S. J. Chen, Z. Xue, W. Withayachumnankul, and C. Fumeaux, "Wideband circularly polarized 3-D printed dielectric rod antenna," *IEEE Trans. Antennas Propag.*, vol. 68, no. 2, pp. 745–753, Feb. 2020, doi: 10.1109/TAP.2019.2943325.

[16] Z. Ji, K. X. Wang, and H. Wong, "Circularly polarized dielectric rod waveguide antenna for millimeter-wave applications," *IEEE Trans. Antennas Propag.*, vol. 66, no. 10, pp. 5080–5087, Oct. 2018, doi: 10.1109/TAP.2018.2858182.

[17] K. Wang, C. Zhang, Y. Shao, and J. Luo, "A broadband circularly polarized endfire loop antenna for millimeter-wave applications," *IEEE Antennas Wireless Propag. Lett.*, vol. 21, no. 7, pp. 1318–1322, Jul. 2022, doi: 10.1109/LAWP.2022.3166767.

[18] J. Wang, Y. Li, L. Ge, J. Wang, M. Chen, Z. Zhang, and Z. Li, "Millimeter-wave wideband circularly polarized planar complementary source antenna with endfire radiation," *IEEE Trans. Antennas Propag.*, vol. 66, no. 7, pp. 3317–3326, Jul. 2018, doi: 10.1109/TAP.2018.2829824.

[19] G. L. Saffold and T. M. Weller, "Dielectric rod antenna array with planar folded slot antenna excitation," *IEEE Open J. Antennas Propag.*, vol. 2, pp. 664–673, 2021, doi: 10.1109/OJAP.2021.3081992.

[20] C. S. Prasad, A. Biswas, and M. J. Akhtar, "Broadband eight-element dielectric rod antenna array using the simple micro-strip slot feeding," *IET Microw., Antennas Propag.*, vol. 13, no. 4, pp. 472–477, Mar. 2019, doi: 10.1049/iet-map.2018.5289.
[21] S. Fakhte and H. Oraizi, "Derivation of the resonant frequency of rectangular dielectric resonator antenna by the perturbation theory," *Appl. Comput. Electromagn. Soc. J. (ACES)*, vol. 31, no. 8, pp. 894–900, 2016.
[22] X. Fang, K. W. Leung, and E. H. Lim, "Singly-fed dual-band circularly polarized dielectric resonator antenna," *IEEE Antennas Wireless Propag. Lett.*, vol. 13, pp. 995–998, 2014, doi: 10.1109/LAWP.2014.2324612.
[23] Y. Shiau, "Dielectric rod antennas for millimeter-wave integrated circuits (short papers)," *IEEE Trans. Microw. Theory Techn.*, vol. MTT-24, no. 11, pp. 869–872, Nov. 1976, doi: 10.1109/TMTT.1976.1128980.
[24] M. Nasir, Y. Xia, M. Jiang, and Q. Zhu, "A novel integrated Yagi–Uda and dielectric rod antenna with low sidelobe level," *IEEE Trans. Antennas Propag.*, vol. 67, no. 4, pp. 2751–2756, Apr. 2019, doi: 10.1109/TAP.2019.2897478.
[25] K.-C. Huang and Z. Wang, "V-band patch-fed rod antennas for high data-rate wireless communications," *IEEE Trans. Antennas Propag.*, vol. 54, no. 1, pp. 297–300, Jan. 2006, doi: 10.1109/TAP.2005.861521.
[26] A. Petosa, *Dielectric Resonator Antenna Handbook*. Norwood, MA, USA: Artech House, 2007.
[27] H. R. Heidari, P. Rezaei, S. Kiani, and M. Taherinezhad, "A monopulse array antenna based on SIW with circular polarization for using in tracking systems," *AEU-Int. J. Electron. Commun.*, vol. 162, Apr. 2023, Art. no. 154563, doi: 10.1016/j.aeue.2023.154563.
[28] P. Sohrabi, P. Rezaei, S. Kiani, and M. Fakhr, "A symmetrical SIW-based leaky-wave antenna with continuous beam scanning from backward-to-forward through broadside," *Wireless Netw.*, vol. 27, no. 8, pp. 5417–5424, Sep. 2021, doi: 10.1007/s11276-021-02798-6.
[29] S. Kiani, P. Rezaei, and M. Fakhr, "On-chip coronavirus shape antenna for wide band applications in terahertz band," *J. Opt.*, vol. 52, no. 2, pp. 860–867, Jan. 2023, doi: 10.1007/s12596-022-01048-y.
[30] S. Kiani and P. Rezaei, "Microwave substrate integrated waveguide resonator sensor for non-invasive monitoring of blood glucose concentration: Low cost and painless tool for diabetics," *Measurement*, vol. 219, Sep. 2023, Art. no. 113232, doi: 10.1016/j.measurement.2023.113232.
[31] S. Kiani, P. Rezaei, and M. Fakhr, "Real-time measurement of liquid permittivity through label-free meandered microwave sensor," *IETE J. Res.*, vol. 11, pp. 1–11, Jul. 2023, doi: 10.1080/03772063.2023.2231875.

SAEED FAKHTE is an Assistant Professor with the Department of Electrical and Computer Engineering, Qom University of Technology, Qom, Iran. His research interests include various areas of antenna engineering, such as graphene antennas, THz antennas, plasmonic antennas, and dielectric antennas.

LADISLAU MATEKOVITS (Senior Member, IEEE) received the degree in electronic engineering from Institutul Politehnic din Bucureşti, Bucharest, Romania, in 1992, and the Ph.D. degree (Dottorato di Ricerca) in electronic engineering from Politecnico di Torino, Turin, Italy, in 1995. Since 1995, he has been with the Department of Electronics and Telecommunications, Politecnico di Torino, first with a Postdoctoral Fellowship and then as a Research Assistant. In 2002, he joined the Department of Electronics and Telecommunications, Politecnico di Torino, as an Assistant Professor. In 2005, he was appointed as a Senior Assistant Professor. In 2005, he was a Visiting Scientist with the Department of Antennas and Scattering, FGAN-FHR (now Fraunhofer Institute), Wachtberg, Germany. In July 2009, he joined Macquarie University, Sydney, NSW, Australia, as a Marie Curie Fellow, for two years, where he also held a visiting academic position, in 2013. In 2014, he was an Associate Professor. In 2014, he was appointed as an Honorary Fellow. In February 2017, he was a Full Professor in Italy. Since 2020, he has been an Honorary Professor with the Polytechnic University of Timisoara, Romania, and an Associate Professor with the Italian National Research Council. He has been invited to serve as a research grant assessor for government funding calls (Romania, Italy, Croatia, Kazakhstan, and Iceland) and as an international expert in Ph.D. thesis evaluation by several universities from Australia, India, Pakistan, and Spain. He has published more than 400 articles, including more than 125 journal contributions, and delivered seminars on these topics all around the world: Europe, USA (AFRL/MIT-Boston), Australia, China, and Russia. His main research interests include numerical analysis of printed antennas and in particular development of new, numerically efficient full-wave techniques to analyze large arrays, and active and passive metamaterials for cloaking applications. Material parameter retrieval of these structures by inverse methods and different optimization techniques has also been considered. In the last years, bio-electromagnetic aspects have also been contemplated, such as example design of implantable antennas or the development of nano-antennas for example for drug delivery applications. He has been a member of the Organizing Committee of the International Conference on Electromagnetics in Advanced Applications (ICEAA), since 2010. He was appointed as a member of the National Council for the Attestation of University Degrees, Diplomas and Certificates (CNATDCU), Romania, from 2020 to 2024. He is a member of the International Advisory Committee and the technical program committee member of several conferences. He was a recipient of various awards in international conferences, including the 1998 URSI Young Scientist Award, Thessaloniki, Greece; the Barzilai Award 1998 (Young Scientist Award, granted every two years by the Italian National Electromagnetic Group); and the Best AP2000 Oral Paper on Antennas, ESA-EUREL Millennium Conference on Antennas and Propagation, Davos, Switzerland. He was a recipient of the Motohisa Kanda Award, in 2018, for the most cited paper of IEEE TRANSACTIONS ON ELECTROMAGNETIC COMPATIBILITY in the past five years. He received the 2019 American Romanian Academy of Arts and Sciences (ARA) Medal of Excellence in Science; the Ad Astra Award, in 2020; a Senior Researcher for Excellence in Research; the Outstanding Associate Editor Award for IEEE ANTENNAS AND WIRELESS PROPAGATION LETTERS, in 2020; and one of the scientists with the highest level of scientific productivity (the top 2% in the world) prepared by Stanford University researchers, in 2022. He has been the Assistant Chairperson and the Publication Chairperson of the European Microwave Week 2002, Milan, Italy; and the General Chair of the 11th International Conference on Body Area Networks (BodyNets 2016). He serves as an Associate Editor for IEEE TRANSACTIONS ON ANTENNAS AND PROPAGATION, IEEE ACCESS, IEEE ANTENNAS AND WIRELESS PROPAGATION LETTERS, and *IET MAP*. He serves as a reviewer for different journals.